nature genetics

Nephrocystin-5, a ciliary IQ domain protein, is mutated in Senior-Loken syndrome and interacts with RPGR and calmodulin

Edgar A Otto[1], Bart Loeys[2], Hemant Khanna[3], Jan Hellemans[4], Ralf Sudbrak[5,6], Shuling Fan[7], Ulla Muerb[1], John F O'Toole[1], Juliana Helou[1], Massimo Attanasio[1], Boris Utsch[1], John A Sayer[1], Concepcion Lillo[8], David Jimeno[8], Paul Coucke[4], Anne De Paepe[4], Richard Reinhardt[5], Sven Klages[5], Motoyuki Tsuda[9], Isao Kawakami[9], Takehiro Kusakabe[9], Heymut Omran[10], Anita Imm[10], Melissa Tippens[11], Pamela A Raymond[11], Jo Hill[12], Phil Beales[12], Shirley He[3], Andreas Kispert[13], Benjamin Margolis[7], David S Williams[8], Anand Swaroop[3,14] & Friedhelm Hildebrandt[1,14]

Nephronophthisis (NPHP) is the most frequent genetic cause of chronic renal failure in children[1–3]. Identification of four genes mutated in NPHP subtypes 1–4 (refs. 4–9) has linked the pathogenesis of NPHP to ciliary functions[9]. Ten percent of affected individuals have retinitis pigmentosa, constituting the renal-retinal Senior-Loken syndrome (SLSN). Here we identify, by positional cloning, mutations in an evolutionarily conserved gene, *IQCB1* (also called *NPHP5*), as the most frequent cause of SLSN. *IQCB1* encodes an IQ-domain protein, nephrocystin-5. All individuals with *IQCB1* mutations have retinitis pigmentosa. Hence, we examined the interaction of nephrocystin-5 with RPGR (retinitis pigmentosa GTPase regulator), which is expressed in photoreceptor cilia and associated with 10–20% of retinitis pigmentosa. We show that nephrocystin-5, RPGR and calmodulin can be coimmunoprecipitated from retinal extracts, and that these proteins localize to connecting cilia of photoreceptors and to primary cilia of renal epithelial cells. Our studies emphasize the central role of ciliary dysfunction in the pathogenesis of SLSN.

The prevalence of NPHP is estimated to be 1 in 100,000, with 1 in 10 affected individuals having retinal dysfunction (SLSN). We identified a cohort of unrelated individuals with NPHP, 435 individuals with isolated kidney involvement and 92 individuals with SLSN. In this cohort, recessive mutations in *NPHP1*, *INVS* (also called *NPHP2*), *NPHP3* or *NPHP4* have so far been detected in only 151 of 435 individuals with NPHP (35%) and in 19 of 92 individuals with SLSN (21%; J. Hoefele & F.H., unpublished data). To identify additional genes causing NPHP and SLSN, we carried out a whole-genome search for linkage in a consanguineous kindred from Turkey (A132), in which linkage to known *NPHP* loci had been excluded. Three children showed the typical clinical features of SLSN (**Fig. 1**). We obtained a significant maximum lod score of $Z_{max} = 3.458$ at marker *D3S1267* on human chromosome 3q21.1 (**Table 1**). By haplotype analysis, we refined the critical genetic region to an interval of 8.7 Mb flanked by markers *D3S1575* and *D3S1551* (**Fig. 1** and **Table 1**). We thereby identified a new locus (*IQCB1*, also called *NPHP5* and *SLSN5*) related to SLSN.

From a total of 57 genes in the critical genetic region, we selected 9 as candidates based on predicted functional domains (**Fig. 2a**). We carried out mutational analysis by direct sequencing of RT-PCR products from Epstein-Barr virus (EBV)-transformed mononuclear cells of two affected individuals of family A132 (VI:1 and IV:5). One of the nine genes, *KIAA0036*, shared two putative IQ calmodulin-binding domains with the *INVS* gene product inversin[9]. In this gene we identified, in kindred A132, a homozygous truncating mutation (nucleotide substitution 1381C→T, corresponding to the amino acid change R461X) that segregated with affected status (**Table 2** and **Fig. 2b**). Mutational analysis by direct sequencing of RT-PCR products of 48 additional individuals with isolated NPHP and 12

[1]Department of Pediatrics, University of Michigan, Ann Arbor, Michigan 48109, USA. [2]McKusick-Nathans Institute for Genetic Medicine, Johns Hopkins University, Baltimore, Maryland 21205, USA. [3]Department of Ophthalmology, University of Michigan, Ann Arbor, Michigan 48109, USA. [4]Center for Medical Genetics, Ghent University Hospital, Ghent 9000, Belgium. [5]Max Planck Institute for Molecular Genetics, Berlin, Germany. [6]Institute for Clinical Molecular Biology, Christian Albrechts University, 24105 Kiel, Germany. [7]Howard Hughes Medical Institute and Department of Internal Medicine, University of Michigan, Ann Arbor, Michigan 48109, USA. [8]Departments of Pharmacology and Neurosciences, School of Medicine, University of California at San Diego, La Jolla, California 92093-0912, USA. [9]Department of Life Science, Graduate School of Life Science, University of Hyogo, Hyogo 678-1297, Japan. [10]University Children's Hospital Freiburg, Freiburg, Germany. [11]Department of Cell and Developmental Biology, University of Michigan, Ann Arbor, Michigan 48109, USA. [12]Molecular Medicine Unit, Institute of Child Health, University College London, London, UK. [13]Institute for Molecular Biology, Medizinische Hochschule Hannover, 30625 Hannover, Germany. [14]Department of Human Genetics, University of Michigan, Ann Arbor, Michigan 48109, USA. Correspondence should be addressed to F.H. (fhilde@umich.edu).

Published online 20 February 2005; doi:10.1038/ng1520

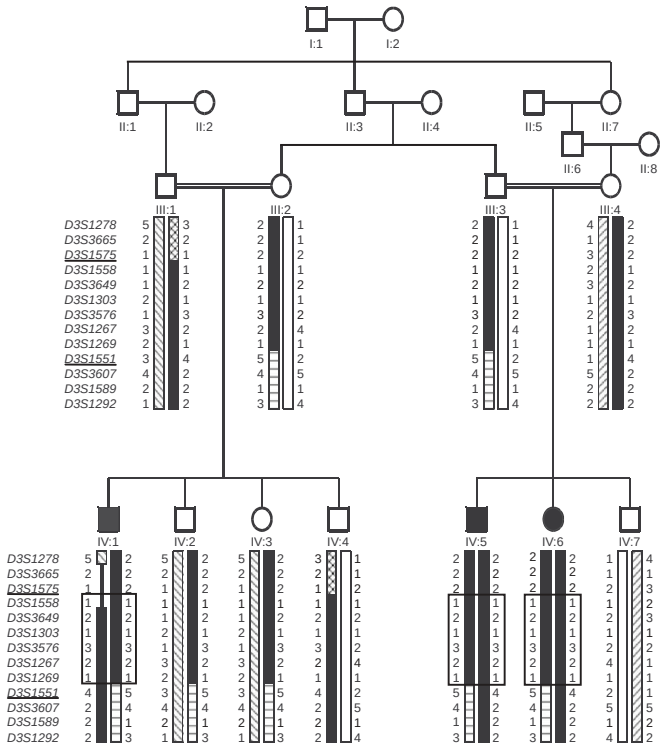

Figure 1 Refinement of the *IQCB1* gene locus by haplotype analysis in the consanguineous pedigree A132 with SLSN. Thirteen microsatellite markers are shown on the left from (top to bottom) centromere to q-arm terminus. Haplotypes are interpreted (differently shaded bars) by minimizing recombinants. Paternal haplotypes are to the left and maternal ones to the right. Segments of haplotypes that could not unambiguously be assigned to the paternal or maternal haplotype are represented by a thin line. A frame depicts the extent of homozygosity by descent. Marker *D3S1575* (underlined) flanks the *IQCB1* locus on its centromeric border, as defined through lack of homozygosity in individual IV:1, and marker *D3S1551* (underlined) flanks the *IQCB1* locus on its telomeric border, as defined through lack of homozygosity in individuals IV:1, IV:5 and IV:6. Flanking markers define a 8.7-Mb critical genetic interval for *IQCB1*. Circles represent females; squares represent males; filled symbols denote the presence of SLSN.

individuals with SLSN yielded three new truncating mutations of *KIAA0036* in 4 unrelated individuals with SLSN. We then carried out mutational screening of all 15 *KIAA0036* exons in 24 additional unrelated individuals with NPHP and 80 unrelated individuals with SLSN. Altogether, we identified eight distinct *KIAA0036* mutations in a total of 16 SLSN individuals from different families (**Table 2** and **Fig. 2b–e**).

Notably, all observed sequence changes were truncating mutations (nonsense mutations, small insertions or deletions), and no missense mutations were detected (**Table 2** and **Fig. 2b–e**). Mutations were detected in exons 6, 9, 11, 13 and 14 (**Table 2** and **Fig. 2b–e**). All individuals with mutations in *KIAA0036* had both NPHP and retinitis pigmentosa, in contrast to individuals with mutations in *NPHP1*, *INVS*, *NPHP3* or *NPHP4*, only 10% of whom have retinitis pigmentosa[8]. Mutational analysis in 72 individuals with NPHP without retinitis pigmentosa detected no mutations. No *IQCB1* mutations were detected in DNA from >155 healthy control individuals. In all cases in which DNA samples were available for testing, all mutations segregated from both parents (**Table 2**). We thus identified *KIAA0036* as a previously unidentified gene causing SLSN type 5. We called this gene *IQCB1* and its gene product nephrocystin-5.

IQCB1 spans 65,676 bp on human chromosome 3 (**Fig. 2a**). It consists of 15 exons. Exons 1 and 2 are not translated. Northern-blot analysis identified a primary transcript of 2.6 kb that is ubiquitously expressed (**Supplementary Fig. 1** online). RNA dot-blot analysis confirmed this pattern in human adult and fetal tissues (data not shown), and *in situ* hybridization detected ubiquitous though weak expression during mouse embryonic development (**Supplementary Fig. 2** online). BLAST analysis of a genomic sequence database of the multicellular model organism *Ciona intestinalis* (sea squirt)[10], using the cDNA of the zebrafish *IQCB1* ortholog as a query, identified a sequence (*cieg034e08*) orthologous to human *IQCB1* (25% amino acid identity). Whole-mount *in situ* hybridization analysis of the *nphp-5* *C. intestinalis* homolog showed ubiquitous expression at all stages of development studied (**Supplementary Fig. 1** online). In contrast with *NPHP1*, *INVS* and *NPHP4* (ref. 11), we could not identify a *C. elegans* ortholog for *IQCB1*.

Table 1 Two-point lod score analysis for the *IQCB1* locus on chromosome 3q13.31–3q21.2

		lod score at θ =						
Marker	Distance (cM)	0.00	0.05	0.10	0.20	0.30	0.40	Z_{max} (θ)
D3S1278		−99.000	0.340	0.702	0.788	0.578	0.264	0.803 (0.15)
D3S3665	0.00	2.103	1.887	1.660	1.181	0.701	0.283	2.103 (0)
D3S1575[a]	2.10	−1.113	0.231	0.367	0.349	0.224	0.091	0.382 (0.15)
D3S1558	2.10	1.636	1.441	1.242	0.839	0.461	0.167	1.636 (0)
D3S3649	0.71	2.048	1.819	1.583	1.100	0.635	0.252	2.048 (0)
D3S1303	1.68	1.618	1.437	1.249	0.861	0.488	0.186	1.618 (0)
D3S3576	1.68	2.879	2.541	2.198	1.508	0.856	0.322	2.879 (0)
D3S1267[b]	1.12	**3.458**[b]	3.097	2.725	1.957	1.189	0.504	**3.458**[b] (0)
D3S1269	0.53	1.576	1.397	1.212	0.832	0.469	0.179	1.576 (0)
D3S1551[a]	0.54	0.189	1.142	1.152	0.877	0.502	0.175	1.152 (0.10)
D3S3607	2.15	−0.134	0.825	0.844	0.614	0.328	0.102	0.844 (0.10)
D3S1589	1.60	−1.526	−0.361	−0.141	0.012	0.042	0.028	0.042 (0.30)
D3S1292	2.66	−0.145	0.836	0.879	0.681	0.389	0.137	0.879 (0.10)

[a]Markers that flank the *IQCB1* critical genetic region within an 8.3-cM genetic and an 8.7-Mb physical map interval are underlined. [b]Maximum lod score and related marker are shown in boldface. Loci compatible with linkage are depicted on a shaded background.

The human full-length *IQCB1* mRNA sequence encodes 598 amino acid residues with a predicted molecular weight of 69 kDa. Analysis of the deduced *IQCB1* sequence yielded a putative coiled-coil domain (amino acids 340–373; **Fig. 2d**), a feature that has also been found in *NPHP1* gene product nephrocystin-1 (ref. 11). In addition, there are two IQ calmodulin-binding regions, at amino acids 294–323 and 387–416, respectively (**Fig. 2d** and **Supplementary Fig. 3** online). This is of interest because the *INVS* gene product inversin also contains two IQ calmodulin-binding regions[9]. To determine whether calmodulin physically interacts with nephrocystin, we carried out a yeast two-hybrid screen of a human fetal brain expression library using a full-length human nephrocystin-5 construct as bait. All 120 positive clones yielded sequences from *CALM*, which encodes calmodulin (data not shown). No other direct binding partners were identified. The interaction of nephrocystin-5 with calmodulin was further confirmed by yeast two-hybrid assay and after switching bait and prey (**Fig. 3a**,**b**). We also carried out yeast two-hybrid assays for other gene products mutated in renal cystic disease. The results were negative for nephrocystins-1, -2, -3 and -4 and for products of genes underlying Bardet-Biedl syndrome (*BBS1–BBS8*; **Fig. 3a**,**b**). We did confirm the known interaction of inversin with calmodulin[12].

To evaluate nephrocystin-5–calmodulin interaction *in vivo*, and to identify additional members of the nephrocystin-5 protein complex, we raised and affinity-purified a polyclonal antibody to a human C-terminal nephrocystin-5 peptide. The antibody recognized a protein of ~55 kDa in extracts of mouse and human retina and mouse kidney (**Supplementary Fig. 4** online). Additional bands in bovine retina probably represent alternatively spliced isoforms. The immunoreactive bands were completely blocked by preincubation with the cognate peptide but not with an irrelevant peptide (**Supplementary Fig. 4** online).

All individuals with *IQCB1* mutations had retinitis pigmentosa in addition to kidney disease. Because nephrocystin-1, nephrocystin-2 and nephrocystin-3 are expressed in primary cilia of renal epithelial cells[8,9], and because mutations in *RPGR* (which is expressed in photoreceptor cilia[13]) cause X-linked retinitis pigmentosa[14,15], we evaluated whether nephrocystin-5 interacts with the main retinal isoform of RPGR-ORF15. We demonstrated coimmunoprecipitation of endogenous nephrocystin-5 from bovine retinal extracts, using an antibody to RPGR-ORF15^{CP} (**Fig. 3c**). Reverse coimmunoprecipitation further confirmed that nephrocystin-5 and RPGR were present in a multiprotein complex in the retina (**Fig. 3d** and **Supplementary Fig. 5** online). The yeast two-hybrid assay did not show an interaction between nephrocystin-5 as bait and either the non-ORF15-containing RPGR isoform (**Fig. 3a**) or the RPGR-ORF15 isoform as prey (data not shown), indicating that nephrocystin-5 and RPGR do not physically interact. We confirmed that the direct nephrocystin-5–calmodulin interaction detected by the direct yeast two-hybrid assay (**Fig. 3a**) also occurred *in vivo* by coimmunoprecipitation from bovine retina extracts (**Fig. 3c**,**d**).

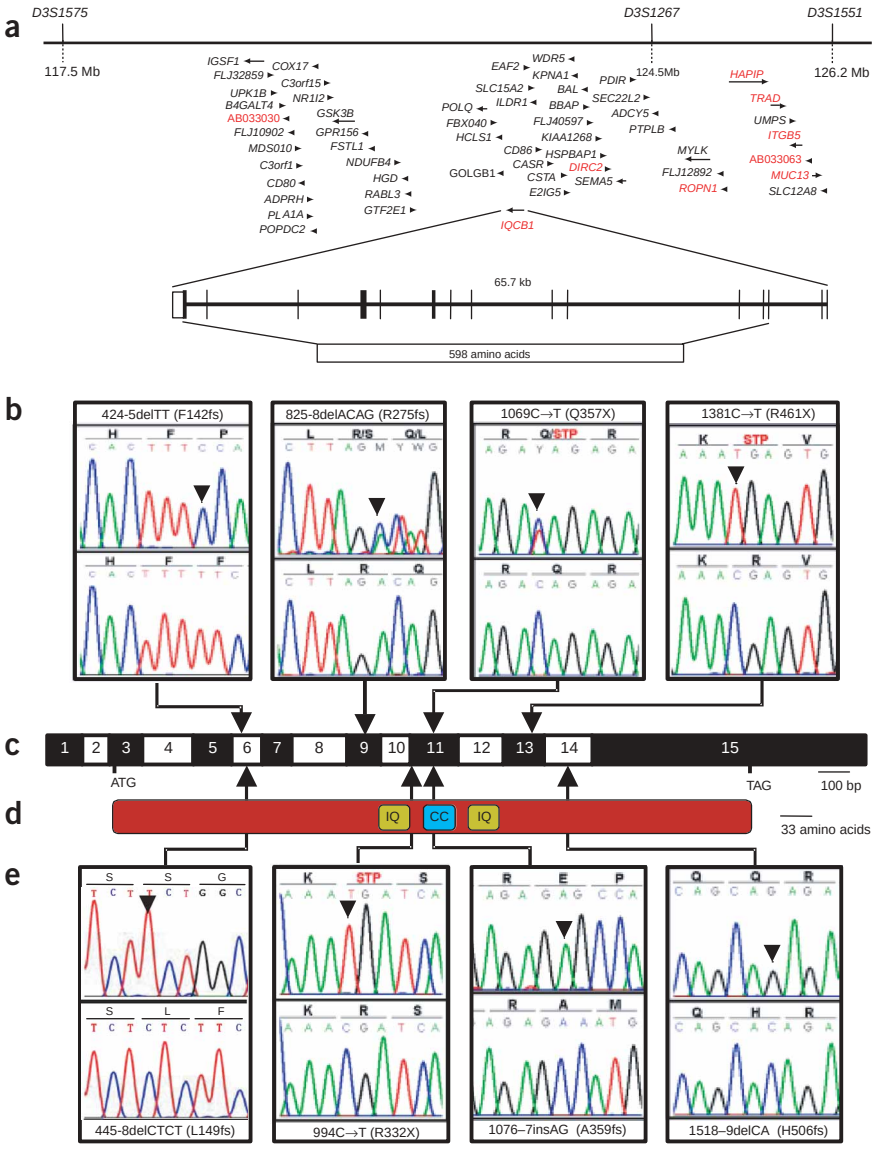

Figure 2 Identification of *IQCB1* by direct mutational analysis in positional candidates. (**a**) The *IQCB1* critical genetic region spanning 8.7 Mb between flanking markers *D3S1575* and *D3S1551* as annotated by GenomeBrowser. Arrows indicate location and transcriptional direction of all 57 positional candidate genes. The cDNAs of genes marked in red were examined by mutation analysis. The exon-intron structure of *KIAA0036* (*IQCB1*) is shown. It encodes 598 amino acids. (**b**,**e**) The eight different *IQCB1* mutations detected in 16 individuals with SLSN (**Table 2**). Sequence traces (nucleotides and respective codons) are shown for affected individuals (top) and healthy controls (bottom). The mutations 825–828delACAG and 1069C→T are shown in the heterozygous state. (**c**) Exon structure of human *IQCB1* cDNA drawn relative to scale bar. Positions of start codon (ATG) at nucleotide +1 and of stop codon (TAG) are indicated. (**d**) Representations of protein motifs are drawn to scale in relation to exon structure. Lines and arrows indicate relative positions of the mutations detected. IQ, IQ calmodulin-binding regions; CC, coiled-coil domain.

Table 2 Mutations in *IQCB1* (*KIAA0036*) detected in 16 persons with SLSN type 5

Family (individual)	Country of origin	Nucleotide alteration(s)[a]	Alteration(s) in coding sequence	Exon (segregation)[b]	Parental consanguinity	Age at ESRD (yr)	Age at RP diagnosis (yr)
F1 (II-1, II-2)	Germany	424–425delTT	F142fsX146	6 (hom, M, nd)	+	15, 12	<3, <3
F399 (II-1)	Germany	424–425delTT	F142fsX146	6 (hom, nd, P)	–	32	0.1
F408 (II-1)	Switzerland	424–425delTT	F142fsX146	6 (hom, nd, nd)	–	8	RP[c]
F409 (II-1)	Switzerland	424–425delTT	F142fsX146	6 (hom, nd, nd)	–	17	RP[c]
F53 (II-2)	Germany	445–448delCTCT	L149fsX179	6 (hom, M, P)	–	16	<1
F269 (II-1)	Germany	445–448delCTCT	L149fsX179	6 (het, nd, nd)	–	37	RP[c]
		825–828delACAG	R275fsX280	9 (het, nd, nd)			
A19 (II-1)	Germany	825–828delACAG	R275fsX280	9 (het, nd, nd)	–	<15	<0.1
		C1069T	Q357X	11 (het, nd, nd)			
F2 (II-1)	Italy	994C→T	R332X	11 (hom, nd, nd)	–	9	0.4
F189 (II-1)	Germany	994C→T	R332X	11 (hom, M, P)	+	<13	RP[c]
F64 (II-3)	North Africa	1076–1077insAG	A359fsX361	11 (hom, M, P)	–	<20	RP[c]
F1146 (II-1, II-2)	Belgium	1076–1077insAG	A359fsX361	11 (hom, M, P)	+	12, >13[d]	0.6, 1.5
A132 (IV-1, IV-5, IV-6)	Turkey	1381C→T	R461X	13 (hom, M, P)	+	<12, <8, <6	0.1, 0.1, 0.1
F50 (II-1, II-3)	Germany	1518–1519delCA	H506fsX518	14 (hom, M, P)	–	12, >13[d]	0.1, 0.1
F54 (II-1)	Germany	1518–1519delCA	H506fsX518	14 (hom, nd, P)	–	<24	RP[c]
F1175 (II-1)	Germany	1518–1519delCA	H506fsX518	14 (hom, M, P)	–	10	0.4
F1298 (II-2)	Germany	1518–1519delCA	H506fsX518	14 (hom, M, P)	–	15	0.1

[a]All mutations were absent from at least 155 healthy control subjects. [b]het, heterozygous in affected individual; hom, homozygous in affected individual; M, mutation identified in mother; P, mutation identified in father; nd, no data or DNA available. [c]Retinitis pigmentosa present but age of onset unknown. [d]Serum creatinine was 2.0 mg dl^{-1} at age 13 years. ESRD, end-stage renal disease; RP, retinitis pigmentosa; yr, years.

Nephrocystins-1, -2, -3 and -4 are expressed in primary cilia of renal epithelial cells (refs. 8,9 and E.A.O., unpublished data). Additionally, virtually all proteins that are encoded by genes that, if mutated, give rise to renal cystic disease are expressed in primary cilia[16]. We therefore investigated whether nephrocystin-5 is similarly expressed in primary cilia of renal epithelial cells (**Fig. 4**). Confocal laser microscopic images of renal epithelial MDCK cells using an antibody to acetylated tubulin marked the primary ciliary tubulin scaffold over its entire length (**Fig. 4a**,**c**,**f**). Nephrocystin-5 localized to these cilia in a dotted staining pattern (**Fig. 4b**,**e**,**f**), in a configuration similar to that of nephrocystin-1 and inversin (also called nephrocystin-2; ref. 9). In addition, calmodulin partially colocalized with both nephrocystin-5 and tubulin, in a punctate pattern (**Fig. 4d–f**). At least one isoform of RPGR-ORF15 is localized in the analogous subcellular structure of the retina, in the photoreceptor connecting cilium and in the outer segment (refs. 13,17 and H.K., unpublished data; **Fig. 4k**). Our data are consistent with the finding that calmodulin is expressed in human photoreceptor connecting cilia[18] and outer segments[19]. We showed by immunofluorescence and immunogold labeling that nephrocystin-5 also localized to the connecting cilia and outer segments of mouse photoreceptor cilia (**Fig. 4g–i**), thereby supporting the idea that it has a role in ciliary functions and interacts with RPGR-ORF15. With sections of mouse retinas, there was significant immunolabeling of the photoreceptor outer segments as well as the connecting cilia (**Fig. 4g–i**), although the only significant immunogold labeling of human retinas was found in the connecting cilium (mean gold particle density ± s.d. on human retinal sections was 1.1 ± 0.7 per μm^2 for photoreceptor outer segments, 5.9 ± 2.7 per μm^2 for connecting cilia and 0.6 ± 0.7 per μm^2 for the retinal pigment epithelium, which represents only background tissue labeling; **Fig. 4j**). In comparing cilia among different tissues, it is important to note that the photoreceptor outer segment represents an amplified distal cilium[20].

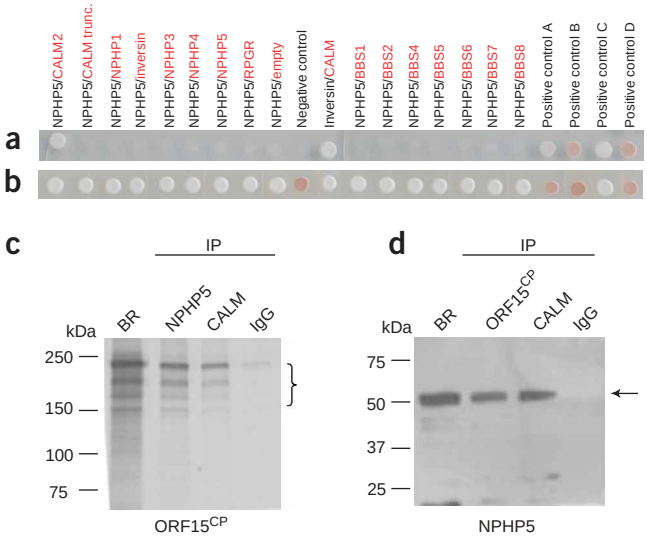

Figure 3 Nephrocystin-5 directly interacts with calmodulin and is complexed with RPGR. (**a**) In yeast two-hybrid direct interaction analysis, nephrocystin-5 (NPHP5) as bait interacts with calmodulin-2 (CALM2) as prey, but not with NPHP1, inversin (also called NPHP2), NPHP3, NPHP4, itself, RPGR, BBS1, BBS2 or BBS4–BBS8 as prey. An empty-vector control is also shown. Inversin interacts with calmodulin[12]. (**b**) Control for colony growth is shown on medium deficient in leucine (–Leu) and tryptophan (–Trp). Red color in certain control colonies is expected to occur upon starvation for specific amino acids. (**c**,**d**) Coimmunoprecipitation of nephrocystin-5 (NPHP5) with RPGR and calmodulin from bovine retinal extracts. Protein extracts from bovine retina (BR; 500 μg) were incubated with antibodies to nephrocystin-5, RPGR-ORF15^{CP} or calmodulin (CALM) or with normal rabbit immunoglobulin (IgG). Immunoblots of the proteins were probed with antibody to RPGR-ORF15^{CP} (**c**) or to nephrocystin-5 (**d**). Bracket in **c** indicates alternatively spliced isoforms of the RPGR protein expressed in the retina[14,23]. Arrow in **d** indicates the specific anti–nephrocystin-5 immunoreactive band.

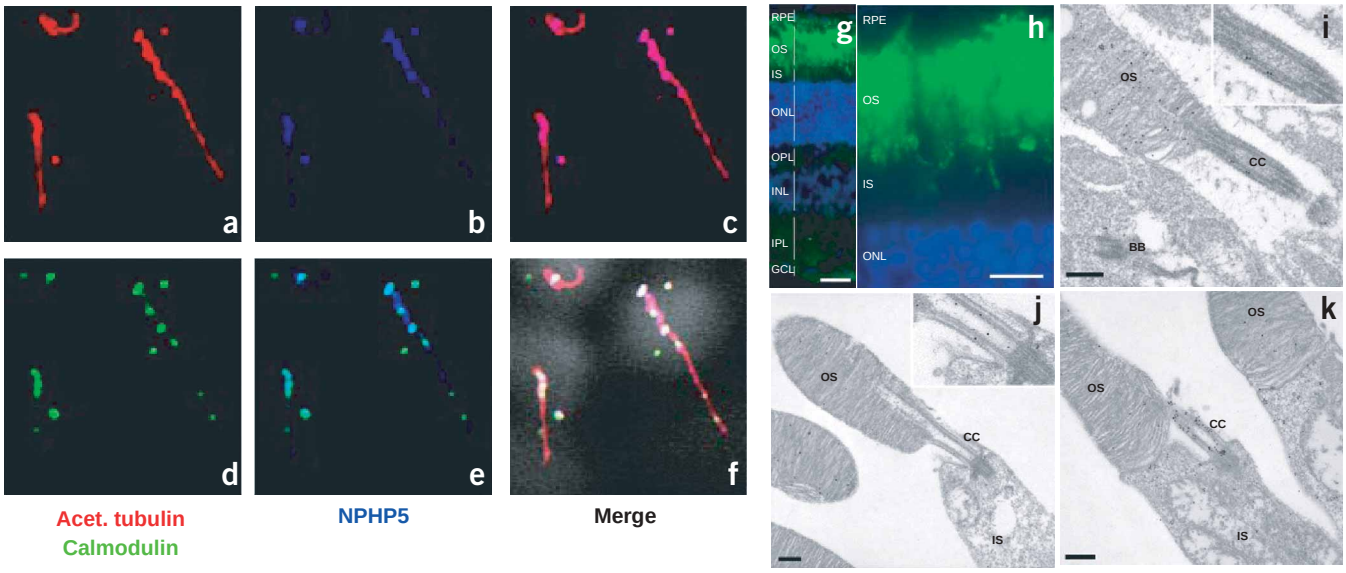

Figure 4 Nephrocystin-5 localizes to primary cilia in renal tubular epithelial cells and retinal cells. (**a**) Acetylated tubulin (red) extends over the entire length of the primary cilia. (**b**) Nephrocystin-5 (NPHP5; blue) is present through most of the length of the primary cilia within punctate varicosities. (**c**) Merged images from **a** and **b** showing localization of nephrocystin-5 (purple) to the primary cilia. (**d**) Calmodulin (green) has a punctate pattern in the primary cilia. (**e**) Merged images from **b** and **d** show that calmodulin staining partially colocalizes with punctate sites of nephrocystin-5 (NPHP5) staining within the primary cilia. Note also labeling of mother and daughter basal bodies. (**f**) Merged images from **a**, **b** and **d** with the addition of DAPI nuclear staining in white. In **a**–**f**, confocal laser microscopy images were captured at the level of the apical membrane. (**g**–**j**) Nephrocystin-5 localizes to the outer segment and connecting cilium of mouse and human photoreceptor cells. Nephrocystin-5 immunofluorescence labeling in mouse retina (green); **h** is a higher magnification of part of **g**. Nuclei are stained blue with DAPI. Also shown is nephrocystin-5 immunogold labeling of mouse (**i**) and human (**j**) photoreceptor cells. Gold particles are evident in the connecting cilium, the outer segment (which is an amplified distal cilium) and the basal bodies. Insets in **i**,**j** show higher magnification of the connecting region of the cilium. (**k**) RPGR immunogold labeling of human photoreceptor cells. Most label is concentrated in the connecting cilium. RPE, retinal pigment epithelium; OS, photoreceptor outer segment(s); CC, connecting cilium; IS, photoreceptor inner segment(s); ONL, photoreceptor nuclei; OPL, photoreceptor synaptic layer; INL, inner nuclear layer; IPL, inner plexiform layer; GCL, ganglion cell layer; BB, basal body. Scale bars: **g**, 25 μm; **h**, 10 μm; **i**–**k**, 300 nm.

Our findings that nephrocystin-5 and RPGR coimmunoprecipitate and share localization to photoreceptors provide molecular evidence for a shared pathogenesis of the kidney and eye phenotypic changes in this renal-retinal syndrome. Because primary cilia of renal epithelial cells and connecting cilia of photoreceptors are homologous subcellular structures, we propose that nephrocystin-5 and RPGR may participate in a common functional pathway of ciliary function. These studies provide a framework for understanding the enigma of ciliary function in kidney as well as in retina. We recently showed that the mouse renal cystic phenotype pcy is caused by mutations in the ortholog of human nephrocystin-3 (ref. 8). As pcy has recently become amenable to treatment with a vasopressin-2 receptor antagonist[21], it will be interesting to evaluate whether the renal and retinal phenotypes of nephrocystin-5 knockout mouse models would likewise be responsive to this treatment.

METHODS

Affected individuals. We obtained blood samples and pedigrees after receiving informed consent from individuals with NPHP and/or their parents and obtained approval for experiments on humans from the University of Michigan Institutional Review Board. In all cases the diagnosis of NPHP was based on the following criteria: (i) clinical course and renal ultrasound or renal biopsy were compatible with the diagnosis of NPHP and/or SLSN as judged by a (pediatric) nephrologist; (ii) the affected individuals had entered end-stage renal disease and (iii) retinitis pigmentosa was diagnosed by an ophthalmologist.

Linkage analysis. We carried out genome-wide homozygosity mapping using the ABI Prism Linkage Mapping Set version 2, consisting of 400 microsatellite markers at an average spacing of 10 cM. We used the MLINK program of the LINKAGE software package to calculate two-point lod scores assuming recessive inheritance with complete penetrance, a disease allele frequency of 0.001 and marker allele frequencies of 0.125.

Mutation analysis. We extracted total RNA from EBV-transformed lymphoblast cell lines from two affected individuals from family A132 using Trizol Reagent (Invitrogen). We carried out RT-PCR using the SuperScript III One-Step RT-PCR System (Invitrogen). We amplified the coding region (according to the University of California Santa Cruz database) of the candidate genes *ROPN1*, *HAPIP*, *TRAD*, *ITGB5*, *MUC13*, *DIRC2*, AB033030, AB033063 and *IQCB1* (*KIAA0036*) and sequenced the RT-PCR products directly on an ABI3700 sequencer (Applied Biosystems). Primer sequences are available on request. After identifying a nonsense mutation in *IQCB1*, we carried out RT-PCR mutational analysis using RNA from EBV-transformed lymphoblast cell lines of 48 individuals with isolated NPHP and 12 with SLSN. In addition, we screened for mutations by amplifying all 15 exons of *IQCB1* by PCR using exon-flanking primers (**Supplementary Table 1** online) in 24 individuals with isolated renal NPHP and 80 individuals with SLSN. Both strands of the PCR products were directly sequenced using the dideoxy chain-termination method on an ABI capillary sequencer. Sequence data were analyzed using Mutation Surveyor (SoftGenetics) and Sequencher software (Gene Codes).

Northern-blot analysis. We purchased a human 12-lane multiple-tissue northern blot and a human multiple-tissue expression array blot from Clontech. As probe, we amplified full-length *IQCB1* cDNA by PCR using cDNA from human mononuclear blood lymphocytes. The probe was radioactively labeled with ^{32}P using the random-primed DNA labeling kit (Roche). Hybridization was at 68 °C overnight in ExpressHyb solution (Clontech). The final washing conditions were 0.1× sodium citrate and 0.1% SDS at 65 °C for 40 min. We

exposed the filters to X-ray film with intensifying screens at −80 °C for 7 d. We used a β-actin cDNA probe as a loading control.

***In situ* hybridization.** We carried out whole-mount *in situ* hybridization using a standard procedure with digoxigenin-labeled antisense riboprobes[22]. The probes used were generated from a 1.9-kb *Iqcb1* mouse cDNA cloned in pCMVSport6 using T7 RNA polymerase. Stained specimens were transferred in 50% glycerol before documentation.

Constructs. Using RT-PCR, we generated human full-length cDNAs of *NPHP1*, *INVS*, *NPHP3*, *NPHP4*, *IQCB1*, *CALM2*, *BBS1*, *BBS2*, *BBS4*, *BBS5*, *BBS6*, *BBS7*, *BBS8* and *RPGR* (non-ORF15-containing isoform) and a cDNA encoding a truncated version of calmodulin (amino acids 1–70) by RT-PCR and cloned them into the Gateway pENTR-TOPO vector (Invitrogen). After LR-clonase recombination, inserts were switched to destination vectors pDEST22 (*Gal4* activation domain–containing yeast two-hybrid vector, Invitrogen) or pDEST32 (*Gal4* binding domain–containing yeast two-hybrid vector, Invitrogen).

Yeast two-hybrid screening. We fused full-length *IQCB1* cDNA to the *Gal4* DNA binding domain in the pDEST32 vector as bait and screened a human fetal brain expression library cloned into the pPC86 *Gal4* activation domain fusion vector (Invitrogen). We screened $\sim 2 \times 10^6$ clones after cotransforming the plasmids into competent MaV203 yeast cells (using the lithium acetate method) and plating the cells on –His, –Leu, –Trp restricted medium. We included 25 mM 3-aminotriazole to suppress leaky growth from *HIS3* mutants. Visible blue-colored yeast colonies grown on plates containing X-α-Gal were analyzed further. Plasmids carried by the transformants were directly sequenced after PCR amplification or plasmid shuffling into *Escherichia coli*. To test for direct yeast two-hybrid interaction of nephrocystin-5 with calmodulin, we cloned the full-length cDNAs corresponding to proteins implicated in NPHP (nephrocystins-1, -2, -3 and -4) or Bardet-Biedl syndrome (BBS1–BBS8) into the pENTR Gateway vector system (Invitrogen) and transferred them to the pDEST22 prey vector or the pDEST32 bait vector. To confirm interaction, we switched inserts from prey to bait vector. Colony growth was compared to those of two negative-control (respective plasmids without insert) and four positive-control yeast strains for different interaction strength, as provided by the kit.

Generation of antibodies to nephrocystin-5 and RPGR. For rabbit immunization, we used a synthetic peptide corresponding to amino acids 566–582 (KKLGEESGDEIDVPKDE) of human nephrocystin-5, whose sequence is identical to that of rat nephrocystin-5 (and has one mismatch with mouse nephrocystin-5). Peptide synthesis, keyhole limpet hemocyanin conjugation and affinity purification of immune serum was done by Washington Biotechnology. The final ELISA titer was 1:100,000,000. Antibody to calmodulin (sc-5537) was from Santa Cruz Biotechnology. This antibody does not discriminate between calmodulin-1, calmodulin-2 and calmodulin-3. (All three human *CALM* gene products are identical in amino acid sequence with the exception of a three–amino acid insertion in calmodulin-3.) Antibody to acetylated tubulin was from Sigma and sheep antibody to CALM was from Bethyl Laboratories. The rabbit polyclonal ORF15^{CP} peptide antibody was generated against the amino acid sequence ^{1100}HKTYQKKSVTNTQGNGKE^{1117} of human RPGR[14]. The antibody was affinity-purified using the cognate peptide. This ORF15^{CP} antibody identified five or six bands with an apparent molecular weight range of 100–250 kDa in mammalian retinas. The bands was abolished by preincubation with 50-fold molar excess of the relevant peptide but not with an irrelevant peptide. In addition, the immunoreactive bands were not detected in the *Rpgr*-knockout mouse retina[13,23] (**Supplementary Fig. 5** online).

Coimmunoprecipitation from bovine retina. We resuspended five bovine retinas in 1× phosphate-buffered saline (PBS) supplemented with Complete protease inhibitor cocktail (Roche) and sonicated them. We centrifuged the sonicate at 10,000*g* for 15 min to remove debris. Immunoprecipitation and subsequent immunoblot analysis was done as described[24].

Immunofluorescence staining of MDCK cells. We seeded MDCK (strain II) cells onto Transwell filters (Corning) and grew them 7 d past confluence. After rinsing them with ice-cold PBS, we fixed cells for 15 min at room temperature with 4% paraformaldehyde in PBS (pH 7.5) and permeabilized them for 5 min at room temperature with 0.1% Triton X-100 in PBS. We washed filters with PBS and then blocked them for at least 1 h in PBS with 2% goat and/or donkey serum. We incubated filters with primary antibodies in blocking solution for at least 2 h, washed them three times in blocking solution at room temperature and then incubated them for 1 h at room temperature with secondary antibodies: Alexa Fluor 488–conjugated donkey antibody to sheep, Alexa Fluor 594–conjugated goat antibody to mouse (Molecular Probes) and Cy5-conjugated goat antibody to rabbit IgG (Jackson ImmunoResearch) with and without primary antibodies as controls. We mounted filters with ProLong antifade kit (Molecular Probes) and obtained confocal images with an Axiovert 100M Zeiss LSM 510 confocal microscope.

Microscopy of retina. For immunofluorescence microscopy, eyes from light-adapted mice were processed and examined as described[25]. For immunoelectron microscopy, eyecups from light-adapted mice and humans were fixed by immersion in 0.1% glutaraldehyde and 2% paraformaldehyde in 0.1 M cacodylate buffer (pH 7.4) and then processed and examined as described[25]. Negative controls included sections from the same retina incubated with 1 mg ml^{-1} of immunogen with the primary antibody.

Gene and protein analysis. We used ClustalW with Jalview for amino acid sequence alignment and ClustalW for multiple protein alignment. To identify known genes, expressed-sequence tags and putative new genes in the critical genomic region, we used National Center for Biotechnology Information Entrez Genome Map Viewer, Ensembl Human Genome Server and GenBank. We obtained the exon-intron boundaries of the *IQCB1* gene (*KIAA0036*) from University of California Santa Cruz.

URLs. ClustalW with Jalview is available at http://zeon.well.ox.ac.uk/git-bin/clustalw.cgi/. ClustalW is available at http://npsa-pbil.ibcp.fr/cgi-bin/npsa_automat.pl?page=npsa_clustalw.html.

Accession numbers. GenBank: human *IQCB1* cDNA, AY714228; mouse *Iqcb1* ortholog, AK078554; *Rattus norvegicus Iqcb1* ortholog, XM_221420; *C. intestinalis Iqcb1* ortholog, AK115136; Ensembl translation ID: *Danio rerio Iqcb1* ortholog, ENSDARP00000004164.

ACKNOWLEDGMENTS

We thank the affected individuals and their families for participation; R.H. Lyons for large-scale sequencing; M. Petry for technical assistance; and G. Feldhoff, T. Bonzel, H.P. Krohn, C.R. Lincke, H. Ruder, M.J. Schuermann, S. Briese, W. Wuyts, A. Raes, Y. Pirson and C. Dahan for contribution of materials and clinical data from affected individuals. This research was supported by grants from US National Institutes of Health to F.H., to A.S. and to D.S.W.; by grants to A.S. from the Foundation Fighting Blindness and Research to Prevent Blindness; and by grants from the German Research Foundation to H.O. F.H. is a Frederick G.L. Huetwell Professor. A.S. is Harold F. Falls Collegiate Professor and recipient of RPB Senior Scientific Investigator Award. B.M. is an investigator of the Howard Hughes Medical Institute. J. Hellemans is funded by the Institute for the Promotion of Innovation by Science and Technology in Flanders. A.K. is supported by grants from the German Research Foundation.

COMPETING INTERESTS STATEMENT

The authors declare that they have no competing financial interests.

Received 4 October 2004; accepted 14 January 2005
Published online at http://www.nature.com/naturegenetics/

1. Smith, C. & Graham, J. Congenital medullary cysts of the kidneys with severe refractory anemia. *Am. J. Dis. Child.* **69**, 369–377 (1945).
2. Fanconi, G., Hanhart, E. & Albertini, A. Die familiäre juvenile Nephronophthise. *Hel. Pediatr. Acta* **6**, 1–49 (1951).
3. Hildebrandt, F. Nephronophthisis—medullary cystic kidney disease. in *Pediatric Nephrology* (eds. Avner, E.D. & Niaudet, P.) 665–673 (Lippincott, Williams & Wilkins, Philadelphia, 2004).
4. Hildebrandt, F. *et al.* A novel gene encoding an SH3 domain protein is mutated in nephronophthisis type 1. *Nat. Genet.* **17**, 149–153 (1997).
5. Saunier, S. *et al.* A novel gene that encodes a protein with a putative src homology 3 domain is a candidate gene for familial juvenile nephronophthisis. *Hum. Mol. Genet.* **6**, 2317–2323 (1997).

6. Otto, E. *et al.* A gene mutated in nephronophthisis and retinitis pigmentosa encodes a novel protein, nephroretinin, conserved in evolution. *Am. J. Hum. Genet.* **71**, 1161–1167 (2002).
7. Mollet, G. *et al.* The gene mutated in juvenile nephronophthisis type 4 encodes a novel protein that interacts with nephrocystin. *Nat. Genet.* **32**, 300–305 (2002).
8. Olbrich, H. *et al.* Mutations in a novel gene, *NPHP3*, cause adolescent nephronophthisis, tapeto-retinal degeneration and hepatic fibrosis. *Nat. Genet.* **34**, 455–459 (2003).
9. Otto, E.A. *et al.* Mutations in *INVS* encoding inversin cause nephronophthisis type 2, linking renal cystic disease to the function of primary cilia and left-right axis determination. *Nat. Genet.* **34**, 413–420 (2003).
10. Dehal, P. *et al.* The draft genome of *Ciona intestinalis*: insights into chordate and vertebrate origins. *Science* **298**, 2157–2167 (2002).
11. Otto, E. *et al.* Nephrocystin gene expression and sequence conservation between human, mouse, and *Caenorhabditis elegans*. *J. Am. Soc. Nephrol.* **11**, 270–282 (2000).
12. Morgan, D. *et al.* The left-right determinant inversin has highly conserved ankyrin repeat and IQ domains and interacts with calmodulin. *Hum. Genet.* **110**, 377–384 (2002).
13. Hong, D.H. *et al.* RPGR isoforms in photoreceptor connecting cilia and the transitional zone of motile cilia. *Invest. Ophthalmol. Vis. Sci.* **44**, 2413–2421 (2003).
14. Vervoort, R. *et al.* Mutational hot spot within a new RPGR exon in X-linked retinitis pigmentosa. *Nat. Genet.* **25**, 462–466 (2000).
15. Breuer, D.K. *et al.* A comprehensive mutation analysis of RP2 and RPGR in a North American cohort of families with X-linked retinitis pigmentosa. *Am. J. Hum. Genet.* **70**, 1545–1554 (2002).
16. Watnick, T. & Germino, G. From cilia to cyst. *Nat. Genet.* **34**, 355–356 (2003).
17. Roepman, R. *et al.* The retinitis pigmentosa GTPase regulator (RPGR) interacts with novel transport-like proteins in the outer segments of rod photoreceptors. *Hum. Mol. Genet.* **9**, 2095–2105 (2000).
18. Cuenca, N. *et al.* The neurons of the ground squirrel retina as revealed by immunostains for calcium binding proteins and neurotransmitters. *J. Neurocytol.* **31**, 649–666 (2002).
19. Chen, T.Y. *et al.* Subunit 2 (or beta) of retinal rod cGMP-gated cation channel is a component of the 240-kDa channel-associated protein and mediates Ca^{2+}-calmodulin modulation. *Proc. Natl Acad. Sci. USA* **91**, 11757–11761 (1994).
20. Besharse, J.C. *et al.* The photoreceptor connecting cilium: a model for the transition zone. in *The Photoreceptor Connecting Cilium: A Model for the Transitions Zone* (ed. Ra, B.) 409–431 (Plenum, New York, 1990).
21. Gattone, V.H. II, Wang, X., Harris, P.C. & Torres, V.E. Inhibition of renal cystic disease development and progression by a vasopressin V2 receptor antagonist. *Nat. Med.* **9**, 1323–1326 (2003).
22. Wilkinson, D.G. Whole mount *in situ* hybridization of vertebrate embryos. in *In Situ Hybridization: A Practical Approach* (ed. Wilkinson, D.G.) 75–84 (Oxford University Press, Oxford, 1992).
23. Hong, D.H. & Li, T. Complex expression pattern of RPGR reveals a role for purine-rich exonic splicing enhancers. *Invest. Ophthalmol. Vis. Sci.* **43**, 3373–3382 (2002).
24. Cheng, H. *et al.* Photoreceptor-specific nuclear receptor NR2E3 functions as a transcriptional activator in rod photoreceptors. *Hum. Mol. Genet.* **13**, 1563–1575 (2004).
25. Gibbs, D. *et al.* Role of myosin VIIa and Rab27a in the motility and localization of RPE melanosomes. *J. Cell Sci.* **117**, 6473–6483 (2004).